

Dynamic modelling of near-surface turbulence in large eddy simulation of wind farms

Jagdeep Singh¹ and Jahrul Alam¹

*Department of Mathematics and Statistics, Memorial University of Newfoundland,
230 Elizabeth Ave, Newfoundland, NL, A1C 5S7, Canada*

Email: alamj@mun.ca

1 ABSTRACT

In large eddy simulation of atmospheric boundary layer flows over wind farms, wall-layer models are generally imposed for the surface fluxes without considering the spatial variability of the surface roughness. In this study, we consider the near-surface model in conjunction with square of the velocity gradient tensor to model the adaptive dissipation of turbulence production. The surface roughness is incorporated through Monin-Obhukhov similarity theory for the computational cells immediately adjacent to the Earth's surface. The underlying proposed near-surface model captures the significant amount of Reynolds stresses in the near-surface and is able to maintain the log-law profile in wind farms. The present study indicates that the suggested 'near-surface model' is relatively robust in comparison to the classical 'near-wall model'.

2 INTRODUCTION

Effects of Coriolis force, atmospheric stability, and meteorological inflow conditions have been extensively studied [8, 31, 21, 11, 45, 47] for wind farms. Generally, equilibrium-contingent models are considered for the surface fluxes ignoring the local variations of the surface roughness. For instance, refs[11, 21] indicates the potential role of local variation of roughness on the performance of wind turbines. In atmospheric boundary layer flows (ABL) over complex terrain, the aerodynamic roughness length (z_0) depends on both the height and distribution of various roughness elements [16]. Local variation of the aerodynamic roughness would have potential influence on the inflow turbulence intensity, thereby, effecting the structural response and power production in the large wind farms [11].

2.1 Literature Review

Typical grid resolutions of large eddy simulation (LES) are insufficient for capturing the dynamic responses of the local variation of roughness of complex terrain [19, 3]. The roughness effect of horizontally homogeneous landscape, for example, grass may be treated with a standard wall-modelling approach [38]. Such wall-modelling techniques are broadly classified into two categories: In the first category, wall-stress models which corrects the velocity gradient at walls through an algebraic relationship between the wall velocity and the velocity at some distance from the wall. The second category combines LES with Reynolds averaged Navier-Stoke's (RANS) equation. In such a hybrid RANS/LES approach, the subgrid model is switched from LES to RANS in close proximity to the wall. The detailed review of both the techniques were done in several studies [e.g. 27, 7, 34, 26]. In literature, there is a lack of sufficient attempts of understanding how to incorporate the effects of local variations of roughness into the wall-stress or hybrid RANS/LES models. Wall-stress models based on Monin-Obhukhov similarity theory often differs in atmospheric boundary layer flows [22, 23, 29, 6, 41] as compared to the engineering applications [43, 34]. In ABL, the log-law is used directly to calculate the local shear stress and imposed an average shear stress computed by LES. This technique have been applied in numerical studies of wind-farms [8, 11, 35].

In this article, we are interested in modelling the transient effect of surface roughness on the near-surface layer of ABL in wind farms. With all the development of wall-layer models for LES, there are still some remaining challenges. First, classification of surface roughness depends on the size and distribution of the roughness elements [44]. For surfaces containing more than one categories of roughness elements,

considering the constant surface flux may not be a good approximation. A complete description of the surface roughness can be found in [39, 16]. Second, a mountainous terrain may contain various roughness elements and it may be complicated to smoothly blend LES with RANS if hybrid RANS/LES model is to be used. Third, such wall-models perform poorly in the presence of relatively large scale obstacles, for example, buildings, topography undulations, and vegetative canopies[38]. Therefore, the shortcomings of LES for ABL flows are often attributed to poor resolution and inadequacy of subgrid model [7].

2.2 Present Work

Wind-farm operates in the surface-layer (10 – 20 %) of the atmospheric boundary layer which accounts for the major portion of turbulent kinetic energy production and dissipation. The flow in wind-farm is considered to be highly turbulent due to spatial variability of surface roughness and interaction of ABL with wind turbines. As the Earth’s surface is approached, the length and time scales considerably decreases and turbulence anisotropy increases. This phenomena is partly resolved by the LES. The vortex-tubes in the surface-layer as well as in close proximity to the surface, are stretched by the principal rate of strain. In the presence of large array of wind turbines, the coherent structures in the surface-layer will also be influenced by wake-vortex interactions. We follow the modern view of Townsend’s attached hypothesis [20, 42] that momentum-carrying eddies near the Earth’s surface are governed by the mean momentum-flux and mean-shear without any explicit dependence on the normal distance to the surface [20]. [10] numerically observed that the stretched vortex-tubes near a surface governs the majority of the wall-shear stress.

In Smagorinsky subgrid scale model, second invariant of the velocity gradient \bar{S}_{ij} is considered. In contrast, we are considering the square of the velocity gradient tensor [24, 1, 4] $\bar{G}_{ij} = (\partial u_i / \partial x_k)(\partial u_k / \partial x_i)$ for the development of near-surface model for the atmospheric turbulence in wind-farms in which eddy viscosity is dynamically computed using rate of strain and rate of rotation. We aim to study a dynamic approach to model surface exchange through dynamic calculation of shear-stress at every grid point adjacent to the Earth’s surface. We propose a methodology which adjusts the eddy viscosity dynamically using second invariant of the square of the velocity gradient tensor, following an additional adjustment of the eddy viscosity arising from the shear stresses due to the surface roughness.

In section 3, we discuss the formulation and implementation of the square of the velocity gradient tensor, near-surface flux and wind-farm modelling. In section 4, numerical assessment of the proposed ‘near-surface’ model is discussed in case of turbulent channel flow, single wind turbine and utility scale wind-farm. Finally, in section 5, we summarize the findings

of the present article.

3 METHODOLOGY

3.1 LES of ABL over wind farms

A large eddy simulation of neutrally stratified ABL flow over wind farms is presented through this work [29, 8, 11, 47]. Atmospheric turbulence around wind farms is characterized by the length scales of the order of 100 m, which may be resolved by the LES approach using a grid space of $\Delta \approx O(10 \text{ m})$. In LES, filtered component of \bar{u}_i is computed by solving the Eq. (1 – 2). When the mesh is sufficiently fine, prediction of turbulence in wind farm is relatively insensitive to the choice of subgrid models for the subfilter scale stresses[32]. The filtered momentum equations,

$$\frac{\partial \bar{u}_i}{\partial t} + \bar{u}_j \frac{\partial \bar{u}_i}{\partial x_j} = -\frac{\partial \bar{p}}{\partial x_i} - \frac{\partial \tau_{ij}}{\partial x_j} + f_i, \quad (1)$$

and the incompressibility condition,

$$\frac{\partial \bar{u}_i}{\partial x_i} = 0, \quad (2)$$

are solved numerically, subject to appropriate boundary conditions. Here, $\bar{u}_i (i = 1, 2, 3)$ are the filtered velocity component. The corresponding wave number is $k_c = 2\pi/\Delta$, where $\Delta = (\Delta x \Delta y \Delta z)^{1/3}$. The sub-filter scale stress tensor in Eq. (1) is defined as $\tau_{ij} = \bar{u}_i \bar{u}_j - \bar{u}_i \bar{u}_j$, and its deviatoric part is represented through the classical Smagorinsky model. i.e. $\tau_{ij}^d = -2\nu_{sgs} \bar{S}_{ij}$. Assuming that the unresolved flow is isotropic, the eddy viscosity is usually given by

$$\nu_{sgs} = C_s \Delta_{les}^2 \sqrt{2\bar{S}_{ij}\bar{S}_{ij}}, \quad (3)$$

where $\bar{S}_{ij} = 1/2(\partial \bar{u}_i / \partial x_j + \partial \bar{u}_j / \partial x_i)$ is the symmetric part of the velocity gradient tensor. An estimate for the Smagorinsky constant is $C_s \approx 0.17$. In ABL flows, the scale of energetic eddies decreases near $z = 0$, where $z = x_3$, is the surface-normal direction. One way to adjust eddy viscosity to the rate of dissipation of near-surface turbulence is to adjust the filter width as $\Delta_{les}^{-2} = [C_s \Delta]^{-2} + [k(z + z_0)]^{-2}$, where $k = 0.41$ is the Von Karman constant, and z_0 is the roughness length. This is a numerical approach that squeezes the spectrum of the resolved flow in the near-surface region. Another method that is commonly employed by the atmospheric sciences research community is the Deardorff model based on turbulent kinetic energy (TKE) [14]. It is necessary to solve the energy transport equation in order to find the subgrid scale TKE, k_{sgs} . If the production of turbulence near $z = 0$ were locally balanced by the rate of dissipation, then k_{sgs} would be adjusted dynamically as the energetic length scales diminishes near $z = 0$. Under these assumptions, the eddy viscosity is defined by

$$\nu_{sgs} = C_s \Delta_{les} k_{sgs}^{1/2}. \quad (4)$$

The models discussed above are designed to account for the flow physics of the atmospheric boundary layer. These

schemes do not directly account for the vortex stretching as well as the flow physics around wind turbines [8]. Surface layer eddies as well as the tip-vortices are stretched by the wind shear. Moreover, interactions among multiple wakes in a large wind farm will enhance the rate of turbulence mixing [21]. Numerical studies of turbulence, however, indicate that vortex stretching [9, 24] as well as the fluctuations of the strain field [18, 40] play a dominant role on the average cascade of TKE from the largest to the smallest scales. Numerical studies reported evidences that strain and vorticity fields of the smallest resolved turbulence fluctuations may be privileged in modelling subgrid scale turbulence [1, 4, 24]. Let us consider the traceless symmetric part of tensor $\mathcal{G}_{ij} = (\partial \bar{u}_i / \partial x_k)(\partial \bar{u}_k / \partial x_j)$ given by $\mathcal{G}_{ij}^d = (1/2)[\mathcal{G}_{ij} + \mathcal{G}_{ji}] - (1/3)\mathcal{G}_{kk}\delta_{ij}$. It can be shown that $\mathcal{G}_{ij}^d \mathcal{G}_{ij}^d = (1/2)|\mathcal{S}\omega|^2 + (2/3)Q^2$, where $\mathcal{S}\omega$ is the vortex stretching vector, $Q = (1/2)(\mathcal{R}_{ij}\mathcal{R}_{ij} - \mathcal{S}_{ij}\mathcal{S}_{ij})$, and $\mathcal{R}_{ij} + \mathcal{S}_{ij} = 2(\partial \bar{u}_i / \partial x_j)$. Thus, the second invariant of the tensor \mathcal{G}_{ij}^d detects strain, rotation, and stretching of vortices. Using a simple dimensional analysis, we express the subgrid-scale TKE dynamically as

$$k_{sgs} = \frac{\Delta_{les}^2 ((1/2)|\mathcal{S}\omega|^2 + (2/3)Q^2)^3}{[(\mathcal{S}_{ij}\mathcal{S}_{ij})^{5/2} + ((1/2)|\mathcal{S}\omega|^2 + (2/3)Q^2)^{5/4}]^2}, \quad (5)$$

Substituting the expression for k_{sgs} given by Eq (5) into the Eq (4), we obtain the eddy viscosity ν_{sgs} that is required to model the deviatoric part of the stress tensor τ_{ij} appeared in Eq (1). To arrive at Eq (5), we compare the expression of the eddy viscosity given in [14] with that given in [24]. The quantity $(\mathcal{G}_{ij}^d \mathcal{G}_{ij}^d)^{3/2}$ varies asymptotically leading to $\nu_{sgs} = O(z^3)$ as $z \rightarrow 0$. This property of \mathcal{G}_{ij}^d is useful for LES of atmospheric turbulence around wind farms, where the viscous layer is often not resolved. The size of the first grid cell adjacent to $z = 0$ is larger than the depth of the viscous sublayer. The eddy viscosity, given by Eq (3-5), is adjusted dynamically in local regions of vortex stretching and strain self-amplification. To evaluate C_w , let us assume that the average rate of dissipation provided by the subgrid model Eq (3-5) is about the same as what would be obtained from the classical Smagorinsky model. Comparing Eq (4) with the expression for the eddy viscosity given by Eq (3), we get

$$C_w = C_s^2 \frac{\sqrt{2\mathcal{S}_{ij}\mathcal{S}_{ij}}}{k_{sgs}^{1/2}}, \quad (6)$$

where k_{sgs} is given by Eq (5) and $C_s = (1/\pi)(3C_k/2)^{-3/4}$.

3.2 Near-surface turbulence and wind-farm modelling

3.2.1 Near-surface flux modelling

In the present work, we consider a situation where the spatial variability of terrain becomes too irregular to be cap-

tured by the immersed boundary method [3] or terrain following method. Consider an equilibrium-contingent wall-stress model based on Monin-Obukhov similarity theory for the smooth surface, the velocity profile may be assumed to satisfy a logarithmic law [13, 43, 27, 26, 5],

$$u(z^+) = u_* \left[\frac{1}{k} \ln(z^+) + C^+ \right], \quad (7)$$

where C^+ is a constant of integration, $z^+ = zu_*/\nu$, is a dimensionless distance, and $u(z^+)$ is the stream wise velocity averaged over a horizontal surface. Eq. (7) can be modified to account for the surface-roughness and Fig 1b shows that flow regimes can be categorized into three categories based on dimensionless characteristic number, $K_s^+ = k_s u_*/\nu$, obtained by scaling the sand-roughness height k_s with viscous length scale δ_ν [25, 33]. This approach may be suitable in the context of the wake-enhanced top-down model of wind farms [15] where one assumes a roughness sub-layer that is characterized by a constant stress and zero pressure gradient ([see 8, 37]).

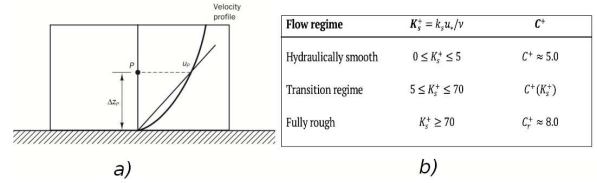


Figure 1: a) Plot shows the first grid cell from the Earth's surface, where, Δz_p is the variation of cell center height from the surface, u_p is the velocity at the cell center. b) Flow regimes based on dimensionless characteristic number (K_s^+) [33].

$$\tau = \nu_{sgs} \frac{u_p}{\Delta z_p}. \quad (8)$$

Wall-stress models based on Eq. (7) assumes a constant value of friction velocity (u_*) on the boundary at $z = 0$, and a boundary condition for τ_{ij} is obtained using Eq.(7). As it can be seen from Fig 1a that this approach is accurate if local variation of wall-shear stress (τ_w) at $z = 0$ is not important. Instead of predicting the land surface fluxes from equilibrium conditions based on the Monin-Obukhov similarity theory [e.g. 6, 2, 22, 38, 46], we consider the local value of u_p at every cell adjacent to the surface which provides a local velocity gradient. Eq. (7) provides a local value of friction velocity (u_*) corresponding to each value of u_p . Considering $u_*^2 = \tau_w$ and $\tau_{ij} = \nu_{sgs} \mathcal{S}_{ij}$, at $z = p$, we correct the value of eddy viscosity (ν_{sgs}). From Fig 1a, it can be clearly seen that if the resolution is not sufficient to capture the gradient, adjusting an eddy viscosity (ν_{sgs}) will correct the shear stress and maintain the log-law. In this approach, one approximates the deviation from the average shear stress, $\tau_w = u_*^2$, as a function of the instantaneous streamwise velocity component, using this formulation, one arrives at the classical wall stress formulation based on the Monin-Obukhov similarity theory; i.e

$\tau_w(x, y, \Delta z_p, t) = c_d u_p u(x, y, \Delta z_p, t)$, where the drag coefficient $c_d = [k/\ln(z_1/z_0)]^2$ and the subgrid scale eddy viscosity ν_{sgs} is adjusted in all grid points adjacent to $z = 0$.

3.2.2 Wind farm modelling

Simulating the details of atmospheric boundary layer flows (ABL) in wind-farms is prohibitively expensive. For example, approximately 30 grid points per actuator line are required to capture the tip-vortices accurately around an individual wind turbine [32]. A comparative study of different parameterization techniques of wind turbine was done by [36] and they reported that actuator disk can accurately represents the wind turbine if one is interested in the main flow structures. In the present study, we consider an actuator disk model where each wind turbine is represented as a local momentum deficit, and thrust force experienced by each turbine is, $f_t = \frac{1}{2} \rho c_t A \langle |u_d| \rangle^2$, where $|u_d| = (1/A) \iint |\bar{\mathbf{u}}| dy dz$ is the average of the instantaneous velocity $\mathbf{u}(x, y, z, t)$ experienced by each rotor, $A = (\pi/4)D^2$ is the area of the rotor. The thrust coefficient of a wake-affected wind turbine is calculated as $c_t = C_T / (1 - a)^2$, where C_T is the thrust coefficient based on the momentum theory [36] and a is the axial induction factor which relates the free stream velocity (u_∞) and the velocity at the rotor disk through $u_\infty = u_d / (1 - a)$.

In the current article, we consider an LES study of atmospheric turbulent flow past an array of 41 wind turbine with the staggered arrangement as shown in Fig 2. The rotor diameter and the hub height of each turbine is $\mathcal{R}_d = 126$ m and $\mathcal{H}_{hub} = 90$, which represents the *REpower* 5-MW turbine [47]. The computational domain $[7048 \times 2880 \times 640]$ m³ is discretized into $624 \times 256 \times 84$ finite volume cells, which is stretched in the vertical direction, thereby, leading to $\Delta z_{min} = 2.29$ m near the bottom boundary, $z = 0$, and $\Delta z_{max} = 11.5$ m near the top boundary ($z = H$). There are 11 grid cells across the rotor in the stream-wise direction.

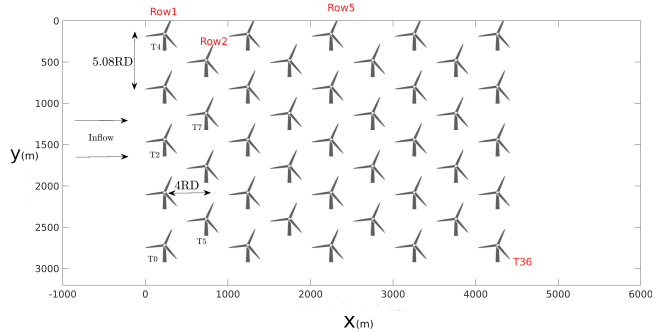


Figure 2: 2D layout of wind farm used for LES simulation, where spanwise and streamwise spacing between turbines are 5.08 and 8 \mathcal{R}_d respectively. \mathcal{R}_d of wind turbine used in this study is 126 m

4 RESULTS AND DISCUSSIONS

4.1 Turbulent channel flow

4.1.1 Direct numerical simulation (DNS) and LES

One can show that [e.g 28, 12], the Reynolds stress of near-surface turbulence depends on local vorticity fluctuations ω' ; i.e.

$$\frac{\partial}{\partial z} \left[\frac{\tau_{13}^R}{\rho} \right] = \left[\overline{u' \times \omega'} \right]_x.$$

In LES, we cannot resolve the vorticity fluctuations near a rough or smooth surface, whereas we expect that the subgrid model accounts for the near-surface fluctuations induced by the remote eddies [28, 12]. DNS results for turbulent flows in channels presumably indicate that fluctuations in both the velocity and the vorticity have been adequately captured. Such fluctuations are not resolved by LES. Here, we consider LES of turbulent channel flows using a grid $192 \times 96 \times 96$ which is stretched in the vertical direction, thereby, leading to $\Delta z_{min} = 5.2 \times 10^{-3}$ m at the bottom boundary, $z = 0$. At a moderate Reynolds number, $Re_b = 13,950$, transitions to the appropriate turbulent regime occur naturally in channel flows [28]. First, we compare the results of LES with that of DNS for a turbulent channel flow [17]. Next, we discuss LES of channel flows on a coarser grid $96 \times 48 \times 48$, where the near-wall resolution is also coarsened by a factor of 5 ($\Delta z_{min} = 2.8 \times 10^{-2}$ m) with respect to the previous simulation on a finer grid $192 \times 96 \times 96$. For the coarser resolution, we consider that the channel walls are rough and the values of the Reynolds number Re_τ are 395, 590, 1000, 2200, and 5200, as shown in Fig 4(a–b). We demonstrate the comparison results to indicate that the present LES bridges the bulk of the channel, dominated by the fluctuations of the strain and vorticity, and the proximity of surfaces with prevailed mean shear. Fig 3a displays the profile of the streamwise mean velocity $u^+ = \langle \bar{u} \rangle / u_*$ as a function of the wall normal distance z^+ . The velocity u^+ is normalized by the wall friction velocity u_* , where the wall-normal distance z^+ is normalized by the length scale $\delta_v = \nu / u_*$ of viscous dissipation. The mean velocity profile exhibits an agreement with the DNS reference data obtained from [17]. In the near-wall region $z^+ \leq 10$, the mean velocity varies like $u^+ = z^+$. In the overlap region, $30 \leq z^+ \leq 300$, the LES data is in a good agreement with the DNS data as well as with the logarithmic profile of the velocity. Fig 3b indicates a slight over prediction of the Reynolds stresses, which may be attributed to the relatively less dissipative numerical scheme, as well as the forcing method, considered in the present work. Nevertheless, the peak value of K.E. (≈ 5) for the LES data has a better agreement with the value reported by [42, 33].

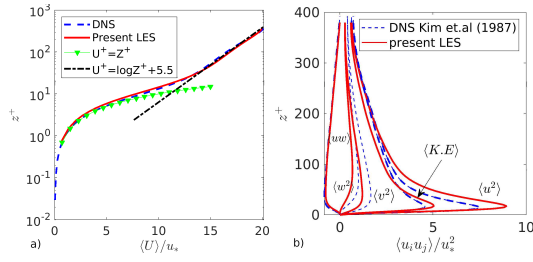


Figure 3: Plot(a-b) first and second order statistics of fully resolved surface-layer in a fully developed turbulent channel flow at $Re_\tau = 395$

4.1.2 Influence of surface roughness

According to Monin-Obukhov similarity theory of the turbulent boundary layer flow, such as $u(z^+) = (1/\kappa) \ln z^+ + C^+$, every surface exhibits some effects of roughness, so that the constant C^+ becomes a function of the roughness length z_0^+ such that $\lim_{z_0^+ \rightarrow 0} C^+(z_0^+) = 5.0$. Here, κ is the von Karman constant, and $z^+ = u_* z / \nu$ is the dimensionless distance from the wall, where u_* is the wall-friction velocity, z measures the wall-normal distance, and ν is the kinematic viscosity. Fig 4 shows that the proposed near-surface model adequately captures the turbulent channel flow.

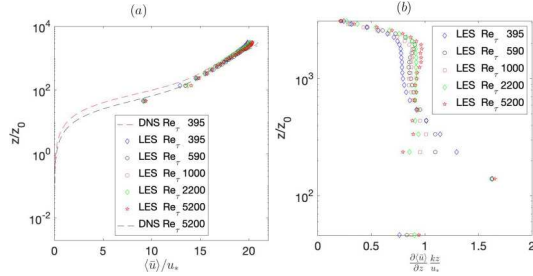


Figure 4: A comparison of the streamwise mean velocity obtained from present LES study with previously reported DNS studies; (a) mean velocity and (b) the wall-normal gradient of the velocity. The values of Reynolds number are $Re_\tau = 395, 590, 1000, 2200$ & 5200 .

4.2 Comparison with reference data: wind tunnel and LES

In LES of atmospheric turbulence over wind farms, resolving the blades is computationally expensive. We consider two dataset to validate the actuator disk model for single wind turbine. We obtained the data from the wind-tunnel experiment conducted by [30] and the LES data for actuator disk model adapted from [36]. Based on the experiment and previous numerical studies, we consider a computational domain of $[5.4 \times 0.9 \times 0.45] m^3$, which is discretized into $256 \times 32 \times 72$ finite volume cells. In this study, we use the

wind turbine model based on [30] with rotor diameter (\mathcal{R}_d) of 0.15 m, hub height (\mathcal{H}_{hub}) of 0.125 m and coefficient of thrust, $C_t = 0.5669$ ($c_t = 0.8248$). Considering the actuator disk approach, we find that the wind turbine wake flow is accurately predicted when the proposed near-surface model is considered. In Fig 5, we observe that there is a good agreement among the present LES and the corresponding LES results [36]. Present LES also shows an average agreement with the wind tunnel measurements[30].

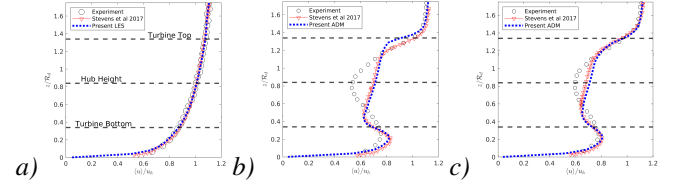


Figure 5: Comparison of mean streamwise velocity at $-1\mathcal{R}_d$, $2\mathcal{R}_d$ and $3\mathcal{R}_d$ respectively of present ADM model with experimental data [30] and LES data [36].

4.3 Interaction of wind farm with ABL

Finally, we consider a LES study for a utility-scale wind farm, the layout of which is depicted in Fig 2. In this simulation, the horizontal grid spacing is approximately 11 m, while the rotor diameter is 126 m. Clearly, such a grid spacing is insufficient to resolve the tip vortices generated by turbines. This section represents how the ABL responds to an array of wind turbines which operate on a fully aerodynamic rough surface. The shear stress exerted by the ABL flow over an aerodynamic rough surface is dominated by the Reynolds stress. In particular the flow near a rough surface accelerates considerably before being retarded by the influence of the turbines. It is necessary that the inlet profiles, the ground shear stress, and the turbulence model should be in equilibrium in close proximity to a rough surface. At the inflow boundary (e.g. $x = -1000$ in Fig 2), we have imposed the undisturbed mean logarithmic profile of ABL flow for the streamwise component of the velocity. On the inlet plane of the computational domain, we have introduced m inviscid large eddies. The strength and intensity of such eddies are chosen randomly in the current study; however, the model is designed in such a way that the strength of such eddies in the inlet plane can be derived from an accompanying meteorological simulation or field measurements, as appropriate.

Fig 6 display the color-filled contour plots of the streamwise instantaneous velocity (Fig 6a), the mean streamwise velocity (Fig 6b), and pressure field (Fig 6c). Fig 6d display the vertical component of vorticity, resolved turbulence kinetic energy (Fig 6e), and resolved fraction of the Reynolds stress (Fig 6f). These color-filled contour plots illustrates the instantaneous flow on the horizontal plane passing through the hub-height $z = 90$ m. Fig 6(a-b) indicates that the first two rows are exposed directly to the wind that was imposed nu-

merically at the inlet boundary $x = -1000$. The asymptotic velocity deficit in rows 2-4 are influenced by the wakes from upstream turbines. The boundary layer is fully developed in the region downstream to row 5. It is worth mentioning that the number of turbines (e.g. 41) and the size of the domain is limited by the computational resources and may not be sufficient to reach a fully developed ‘large wind-farm’. Such limitations are to be considered while interpreting our LES data. Nevertheless, the overall flow pattern is consistent with the expected regime of turbulent flow over fully developed wind farms.

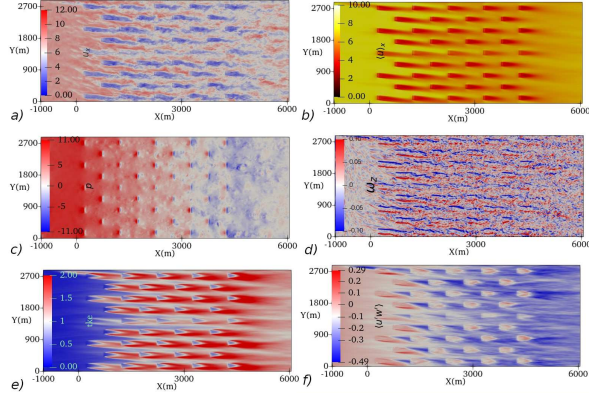


Figure 6: Color filled contour plots based on proposed near-surface model in conjunction with square of the velocity gradient sgs model on a $x - z$ plane cutting through the hub height $\mathcal{H}_{hub} = 90$ m of the turbines a) u_x , instantaneous stream-wise velocity b) $\langle u_x \rangle$, mean stream-velocity c) Pressure field, d) ω_z , vorticity in the surface normal direction e) TKE, turbulent kinetic energy and f) $\langle u'w' \rangle$, vertical flux.

Fig 7a shows that the vertical profile of the velocity agrees with the logarithmic profile in regions below and above the wind turbine array. Moreover, the velocity deficit in Fig 7 exhibits a close agreement with the corresponding profile of wind tunnel measurement depicted in Fig 5b. Fig 7b shows the profile of velocity deficit, where the classical near-wall model is employed.

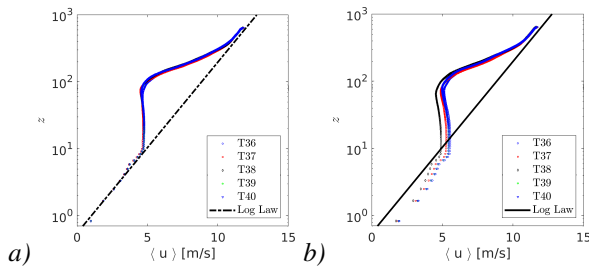


Figure 7: A comparison of velocity deficit behind the wind turbines in utility-scale wind farm. (a) proposed near-surface model. (b) classical wall-stress model for rough-surface ABL [22].

In order to understand the influence of inflow turbulence, Fig 8 compares the energy spectrum with respect to the two turbulence models. A theoretical $-5/3$ slope proposed by Kolmogorov and Kaimal spectra is considered to verify the capability of LES model to reproduce the energy cascade.

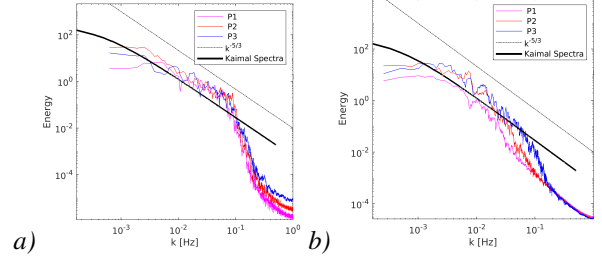


Figure 8: Energy spectra of streamwise velocity captured at P1(716, 1440, 27), P2(2732, 1440, 27) and P3(4244, 1440, 27). a) Proposed near-surface model in conjunction with square of the velocity gradient sgs model. b) A subgrid model commonly used in ABL flow simulation [e.g., TKE-1.5 model, 14].

In Fig 9, we consider the wavelet coherency diagram for the wind around the turbine #1 (see layout in Fig 2). We employed the wavelet transform technique to understand the role of coherent structures in the wind farm. In comparison to fourier transform, wavelet transform can extract both local spectrum and temporal details. It can be clearly seen from the Fig 9b that energy spectrum is associated with the transient coherent vortices.

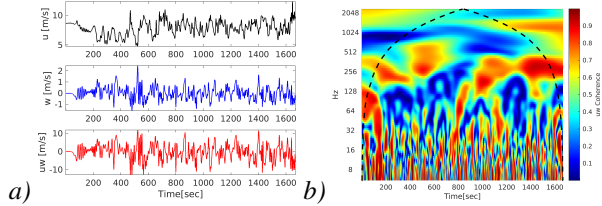


Figure 9: a) Instantaneous vertical flux. b) wavelet power spectral density of the vertical flux captured at P1(716, 1440, 163).

5 CONCLUSION

We have developed a dynamic procedure of modeling sub-grid scale near-surface atmospheric turbulence in large wind farms. This approach resolves neither the near-surface region nor the wind turbine blades. A salient feature is the dynamic blending of shear stress, while implementing the Dirichlet boundary conditions. In this model the scaling of the eddy viscosity is achieved dynamically, which is based on the vortex stretching vector, instead of the classical scaling Δ^2 , where Δ is the grid spacing. Unlike the classical dynamic approach of modelling subgrid scale stress, the fraction of the desired level of dissipation is fixed through a global

value of the model parameter C_w . However, the exchange of momentum between the earth's surface and the atmosphere aloft assumes a local dynamic variation of Monin-Obukhov similarity profile at each grid point adjacent to the surface.

In comparison to classical wall-stress model for rough wall atmospheric turbulence combined with a kinetic energy based subgrid model (commonly utilized in atmospheric boundary layer studies), the results indicate that the new model is capable to accurately predict both the wind turbine wake dynamics and the near-surface atmospheric turbulence. It is also observed that the energy spectrum follows the classical power law $k^{-5/3}$ in case of the proposed model, exhibiting a 'sharp spectral cutoff' although we have considered a finite-volume discretization. Using wavelet coherency diagram, we observe that the energy spectrum is indeed associated with the transient coherent vortices.

We plan to discuss further advancement of this development in another article, which is currently in progress. In particular, the underlying symmetries of the differential operators are preserved in the numerical scheme that we have implemented within our in-house LES code. Although the actuator disk approach is considered, we are working on improved modelling of the thrust of wind turbines through the advancement of the canopy-stress model in the individual wake of turbines in large wind farms. Canopy-stress model is considered to be an effective numerical tool to model ABL, as well as the effects of mountain-like obstacles in the atmospheric boundary layer.

REFERENCES

- [1] J. M. Alam and L. P. Fitzpatrick. Large eddy simulation of flow through a periodic array of urban-like obstacles using a canopy stress method. *Computers & Fluids*, 171:65–78, 2018.
- [2] R. S. Arthur, J. D. Mirocha, K. A. Lundquist, and R. L. Street. Using a canopy model framework to improve large-eddy simulations of the neutral atmospheric boundary layer in the weather research and forecasting model. *Monthly Weather Review*, 147(1):31–52, 2019.
- [3] J. Bao, F. K. Chow, and K. A. Lundquist. Large-eddy simulation over complex terrain using an improved immersed boundary method in the weather research and forecasting model. *Monthly Weather Review*, 146(9):2781–2797, 2018.
- [4] M. A. S. Bhuiyan and J. M. Alam. Scale-adaptive turbulence modeling for les over complex terrain. *Engineering with Computers*, pages 1–13, 2020.
- [5] S. T. Bose and G. I. Park. Wall-modeled large-eddy simulation for complex turbulent flows. *Annual review of fluid mechanics*, 50:535–561, 2018.
- [6] J. G. Brasseur and T. Wei. Designing large-eddy simulation of the turbulent boundary layer to capture law-of-the-wall scaling. *Physics of Fluids*, 22(2):021303, 2010.
- [7] W. Cabot and P. Moin. Approximate wall boundary conditions in the large-eddy simulation of high reynolds number flow. *Flow, Turbulence and Combustion*, 63(1):269–291, 2000.
- [8] M. Calaf, C. Meneveau, and J. Meyers. Large eddy simulation study of fully developed wind-turbine array boundary layers. *Physics of fluids*, 22(1):015110, 2010.
- [9] M. Carbone and A. D. Bragg. Is vortex stretching the main cause of the turbulent energy cascade? *Journal of Fluid Mechanics*, 883:R2, 2020.
- [10] D. Chung and D. Pullin. Large-eddy simulation and wall modelling of turbulent channel flow. *Journal of fluid mechanics*, 631:281–309, 2009.
- [11] M. J. Churchfield, S. Lee, J. Michalakes, and P. J. Moriarty. A numerical study of the effects of atmospheric and wake turbulence on wind turbine dynamics. *Journal of turbulence*, (13):N14, 2012.
- [12] P. A. Davidson. *Turbulence: an introduction for scientists and engineers*. Oxford university press, 2015.
- [13] J. W. Deardorff. A numerical study of three-dimensional turbulent channel flow at large reynolds numbers. *Journal of Fluid Mechanics*, 41(2):453–480, 1970.
- [14] J. W. Deardorff. Numerical investigation of neutral and unstable planetary boundary layers. *Journal of Atmospheric Sciences*, 29(1):91–115, 1972.
- [15] S. Frandsen, R. Barthelmie, S. Pryor, O. Rathmann, S. Larsen, J. Højstrup, and M. Thøgersen. Analytical modelling of wind speed deficit in large offshore wind farms. *Wind Energy: An International Journal for Progress and Applications in Wind Power Conversion Technology*, 9(1-2):39–53, 2006.
- [16] J. Garratt. *The Atmospheric Boundary Layer*. Cambridge University Press, 1994.
- [17] J. Kim, P. Moin, and R. Moser. Turbulence statistics in fully developed channel flow at low reynolds number. *Journal of fluid mechanics*, 177:133–166, 1987.
- [18] E. L  v  que, F. Toschi, L. Shao, and J. P. Bertoglio. Shear-improved smagorinsky model for large-eddy simulation of wall-bounded turbulent flows. In *Fifth International Symposium on Turbulence and Shear Flow Phenomena*. Begel House Inc., 2007.
- [19] K. A. Lundquist, F. K. Chow, and J. K. Lundquist. An immersed boundary method enabling large-eddy simulations of flow over complex terrain in the wrf model. *Monthly Weather Review*, 140(12):3936–3955, 2012.

- [20] I. Marusic and J. P. Monty. Attached eddy model of wall turbulence. *Annual Review of Fluid Mechanics*, 51:49–74, 2019.
- [21] C. Meneveau. The top-down model of wind farm boundary layers and its applications. *Journal of Turbulence*, (13):N7, 2012.
- [22] C.-H. Moeng. A large-eddy-simulation model for the study of planetary boundary-layer turbulence. *Journal of the Atmospheric Sciences*, 41(13):2052–2062, 1984.
- [23] C.-H. Moeng and P. P. Sullivan. A comparison of shear-and buoyancy-driven planetary boundary layer flows. *Journal of Atmospheric Sciences*, 51(7):999–1022, 1994.
- [24] F. Nicoud and F. Ducros. Subgrid-scale stress modelling based on the square of the velocity gradient tensor. *Flow, turbulence and Combustion*, 62(3):183–200, 1999.
- [25] J. Nikuradse et al. Laws of flow in rough pipes. 1950.
- [26] U. Piomelli. Wall-layer models for large-eddy simulations. *Progress in aerospace sciences*, 44(6):437–446, 2008.
- [27] U. Piomelli and E. Balaras. Wall-layer models for large-eddy simulations. *Annual review of fluid mechanics*, 34(1):349–374, 2002.
- [28] S. B. Pope. *Turbulent flows*. IOP Publishing, 2001.
- [29] F. Porté-Agel, C. Meneveau, and M. B. Parlange. A scale-dependent dynamic model for large-eddy simulation: application to a neutral atmospheric boundary layer. *Journal of Fluid Mechanics*, 415(ARTICLE):261–284, 2000.
- [30] F. Porté-Agel, Y.-T. Wu, H. Lu, and R. J. Conzemius. Large-eddy simulation of atmospheric boundary layer flow through wind turbines and wind farms. *Journal of Wind Engineering and Industrial Aerodynamics*, 99(4):154–168, 2011.
- [31] S. B. Roy. Simulating impacts of wind farms on local hydrometeorology. *Journal of Wind Engineering and Industrial Aerodynamics*, 99(4):491–498, 2011.
- [32] H. Sarlak, C. Meneveau, and J. N. Sørensen. Role of subgrid-scale modeling in large eddy simulation of wind turbine wake interactions. *Renewable Energy*, 77:386–399, 2015.
- [33] H. Schlichting and K. Gersten. *Boundary-layer theory*. Springer, 2016.
- [34] I. Senocak, A. S. Ackerman, M. P. Kirkpatrick, D. E. Stevens, and N. N. Mansour. Study of near-surface models for large-eddy simulations of a neutrally stratified atmospheric boundary layer. *Boundary-layer meteorology*, 124(3):405–424, 2007.
- [35] R. J. Stevens, J. Graham, and C. Meneveau. A concurrent precursor inflow method for large eddy simulations and applications to finite length wind farms. *Renewable energy*, 68:46–50, 2014.
- [36] R. J. Stevens, L. A. Martínez-Tossas, and C. Meneveau. Comparison of wind farm large eddy simulations using actuator disk and actuator line models with wind tunnel experiments. *Renewable energy*, 116:470–478, 2018.
- [37] R. J. Stevens, M. Wilczek, and C. Meneveau. Large-eddy simulation study of the logarithmic law for second and higher-order moments in turbulent wall-bounded flow. *arXiv preprint arXiv:1405.0950*, 2014.
- [38] R. Stoll, J. A. Gibbs, S. T. Salesky, W. Anderson, and M. Calaf. Large-eddy simulation of the atmospheric boundary layer. *Boundary-Layer Meteorology*, 177(2):541–581, 2020.
- [39] R. B. Stull, C. D. Ahrens, et al. *Meteorology for scientists and engineers*. Brooks/Cole, 2000.
- [40] P. P. Sullivan, J. C. McWilliams, and C.-H. Moeng. A subgrid-scale model for large-eddy simulation of planetary boundary-layer flows. *Boundary-Layer Meteorology*, 71(3):247–276, 1994.
- [41] P. P. Sullivan and E. G. Patton. The effect of mesh resolution on convective boundary layer statistics and structures generated by large-eddy simulation. *Journal of the Atmospheric Sciences*, 68(10):2395–2415, 2011.
- [42] A. Townsend. *The structure of turbulent shear flow*. Cambridge university press, 1980.
- [43] H. Versteeg and W. Malalasekera. Computational fluid dynamics: the finite volume method. *Harlow, England: Longman Scientific & Technical*, 1995.
- [44] J. Wieringa. Updating the davenport roughness classification. *Journal of Wind Engineering and Industrial Aerodynamics*, 41(1-3):357–368, 1992.
- [45] Y.-T. Wu and F. Porté-Agel. Simulation of turbulent flow inside and above wind farms: model validation and layout effects. *Boundary-layer meteorology*, 146(2):181–205, 2013.
- [46] H. Wurps, G. Steinfeld, and S. Heinz. Grid-resolution requirements for large-eddy simulations of the atmospheric boundary layer. *Boundary-Layer Meteorology*, pages 1–23, 2020.
- [47] S. Xie and C. L. Archer. A numerical study of wind-turbine wakes for three atmospheric stability conditions. *Boundary-Layer Meteorology*, 165(1):87–112, 2017.